

## Microstructural analysis using X-ray computed tomography (CT) in flax/epoxy composites

M Kersani<sup>1,2</sup>, SV Lomov<sup>2</sup>, AW Van Vuure<sup>2</sup>, A Bouabdallah<sup>1</sup> and I Verpoest<sup>2</sup>

<sup>1</sup>Faculty of Physics, University of Science and Technology Houari Boumediene, Algiers, Algeria

<sup>2</sup>Department of Metallurgy and Materials Engineering, KU Leuven, Leuven, Belgium

E-mail: kersani.malika@gmail.com

**Abstract.** Among natural fibres which have recently become attractive to researchers, flax is probably the most commonly used bast-type fibre today. Due to its properties and availability, flax fibre has potential to substitute glass in polymer composites. A flax fibre has a complex structure; it can be classified into elementary fibres, which are grouped into so-called technical fibres. These technical fibres themselves are actually composite structures. Several works [1, 2, 3] were focussed on the study of damage behaviour in unidirectional flax fibres reinforced composites, where materials were subjected to tensile loading. At the microscopic level and at low stress, microcracks arise within the material and by growing they may lead to other forms of damage such as delamination, fibre breakage, interfacial debonding...etc. In order to better understand the damage phenomena and to better control the parameters which lead to the failure, several methods and techniques have been developed on natural fibre reinforced composites [2, 3]. In the present work, X-ray computed tomography (CT) technique has been used to observe damage in flax/epoxy quasi-unidirectional woven laminates, loaded in uniaxial tension. The tensile tests show that these composites offer good mechanical properties. X-ray computed tomography technique allowed us, on the one hand to determine the microstructure parameters of the studied composites and to observe the damage occurring during loading, on the other. The inspection of the several tomography images showed cracks on interface of the yarns and technical fibres.

### 1. Introduction

Micromechanics damage in laminates commonly initiates with transverse matrix cracking in 90° plies, when loaded in tension. Experimental recent study performed on natural fibre reinforced composites: flax/epoxy [4], didn't reveal such cracks till the late stage of loading. In this previous study, different laminates were subjected to tensile loading then analyzed under an optical microscopy, at different stages of loading. To go deeper in the structure, in the present work samples prepared from similar laminates were subjected to tension then analysed by the X-ray computed tomography (CT). CT analysis is a useful method in finding eventual internal cracks that are not visible by optical microscopy.



## 2. Materials and methodology

The material used in this work is a quasi-unidirectional woven preregs, flax/epoxy, with areal density of the reinforcement 170 g/m<sup>2</sup>, provided by LINEO (Belgium). The woven fabric is pre-impregnated with epoxy resin (prepreg system Araldite LY5150/Aradur 1571/Accelerator 1573/HardenerXB3471). The quasi-unidirectional woven preregs is made of flax fibres oriented in the warp direction (95.5%) and 4.5% flax fibres in the weft direction (see figure 1). All the studied laminates are constituted of eight layers of the flax prepreg. The orientation in each laminate is made symmetrically to its middle plan. Figure 2 illustrated the sequence of the layers in each laminate. 0° direction is defined as the direction parallel to the loading. The angle in the designation of the laminate means warp orientation of the corresponding fabric layer.

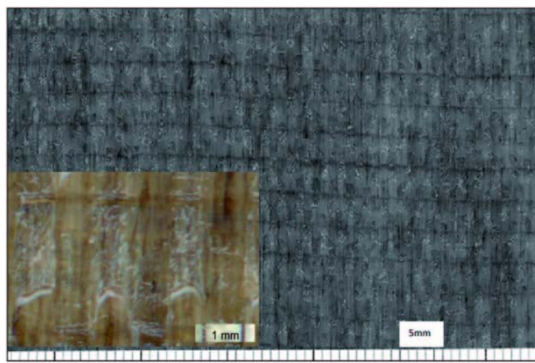


**Figure 1.** Flax prepreg. Warp direction is vertical. Insert: enlarged image.

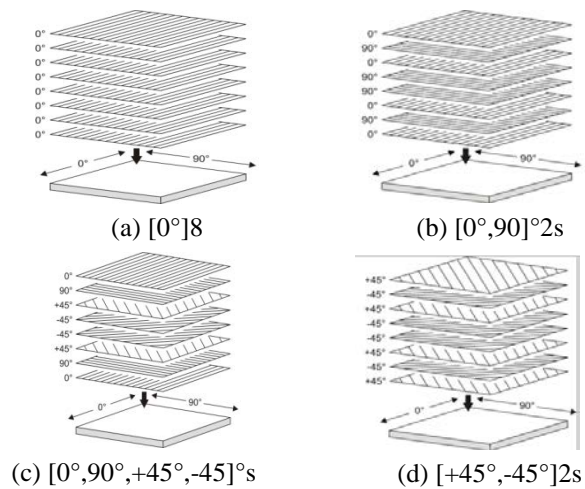


**Figure 2.** The different architectures of the prepared composites.

Several plates with different lay-up configurations:  $[0^\circ]_8$ ,  $[0^\circ, 90^\circ]_{2s}$ ,  $[0^\circ, 90^\circ, +45^\circ, -45^\circ]_s$  and  $[+45^\circ, -45^\circ]_{2s}$  were prepared using vacuum bag and an autoclave. The temperature and the pressure during autoclaving reached 130°C and 4 bars, respectively. The total fibre volume fraction of all the laminates is  $47 \pm 2\%$ .

## 3. Results and discussion

### 3.1 Optical microscopy observations

In order to analyze the plate's cross sections specimens of 1x1 cm were cut from the plates' edges; these cross sections, observed under an optical microscope, are shown in figure 3.

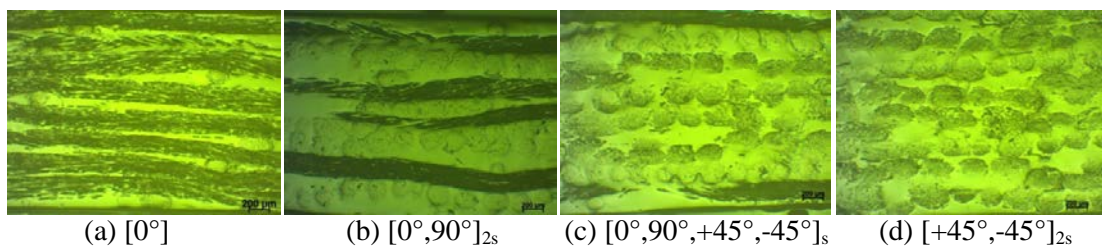


**Figure 3.** Optical microscopy showing the cross sections of the laminates (sections parallel to 0° axis).

These micrographs highlight the different sequences of the laminates and reveal also a good quality of impregnation: no voids were revealed from the optical microscopy observation, in all of the prepared laminates, at the external surface level.

### 3.2 X-ray computed tomography (CT) of the virgin samples

To go somewhat deeper into the structure and in the attempt to visualize eventual defects, X-ray computed tomography (CT) technique was adopted. The CT method was performed with a Phoenix Nanotom using VGStudio software. The target material used in the tube was tungsten and the exposure conditions were 69 kV and 150  $\mu$ A. Samples with size 10X10 mm were cut from the prepared plates and then exposed to X-ray beam under different angular positions.

From a large number of the recorded two-dimensional X-ray projection images, the three dimensional (3D) image (figure 4) of the sample is then computationally reconstructed. From the 3D images of the different structures, 2D slices in any plane (x-y, x-z and y-z planes) can be observed. An example of these structures can be seen in figure 5.

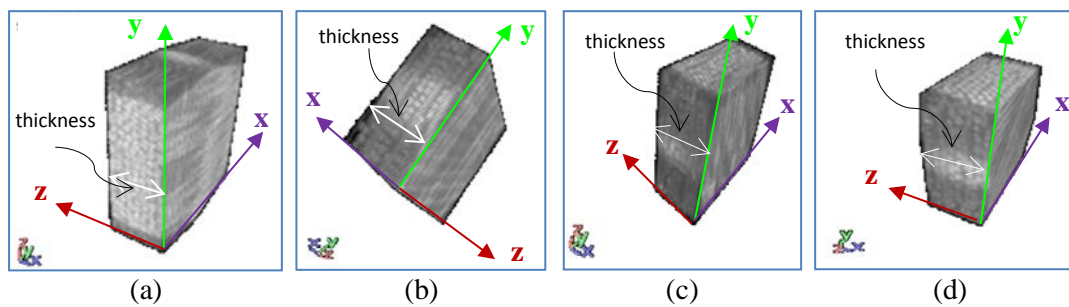


**Figure 4.** Tomography image illustrating the reconstructed 3D volume of (a)  $[0^\circ]_8$ , (b)  $[0^\circ, 90^\circ]_{2s}$ , (c)  $[0^\circ, 90^\circ, +45^\circ, -45^\circ]_s$  and (d)  $[+45^\circ, -45^\circ]_{2s}$ . (Y axis is parallel to the  $0^\circ$  direction).

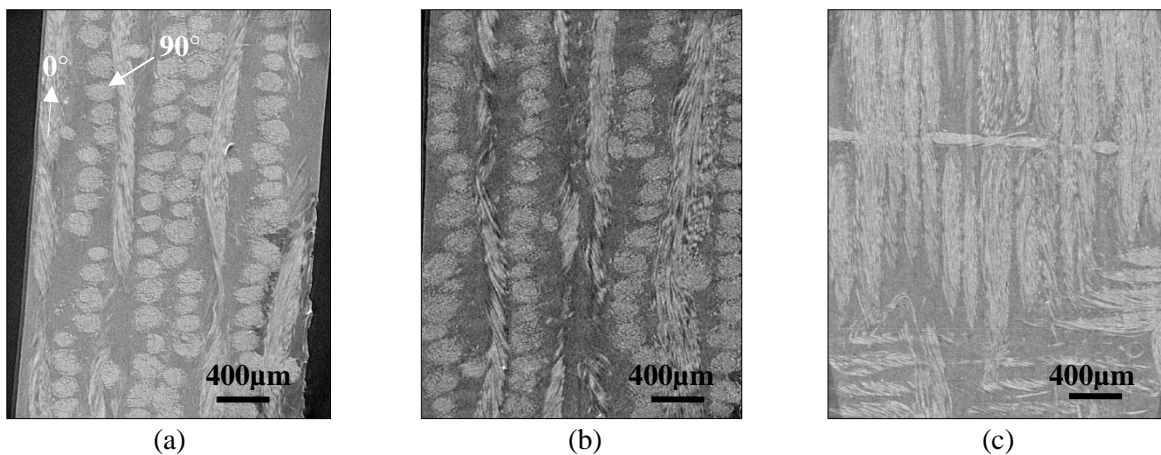
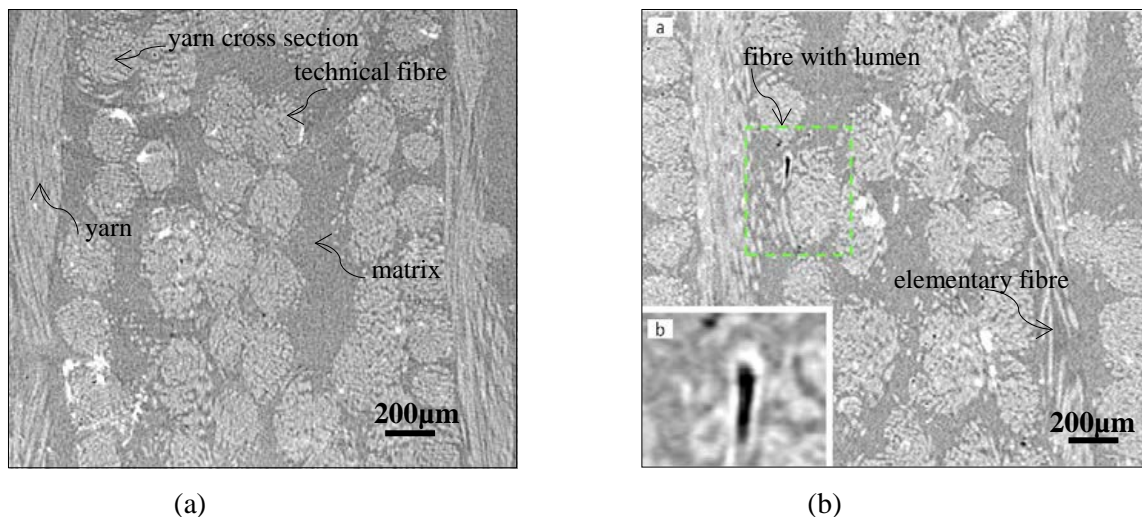


**Figure 5.** Internal 2D slice in a scanned 3D volume of  $[0^\circ, 90^\circ]_{2s}$  laminate. (a) In x-y plane, (b) in x-z plane and (c) in y-z plane (y axis is parallel to  $0^\circ$  axis).

The inspection on the several 2D tomographs allowed us to determine the microstructural parameters of the studied composites. Figure 6 shows an example of internal 2D slice in a scanned 3D volume, relative to  $[0^\circ, 90^\circ, +45^\circ, -45^\circ]_s$  structure, in its unloaded state. In this figure the different microstructural characteristics are illustrated. The left image shows 2D slice in x-y plane, where the yarn cross sectional structure can be observed. The yarn about 200-500  $\mu$ m, is constituted of an

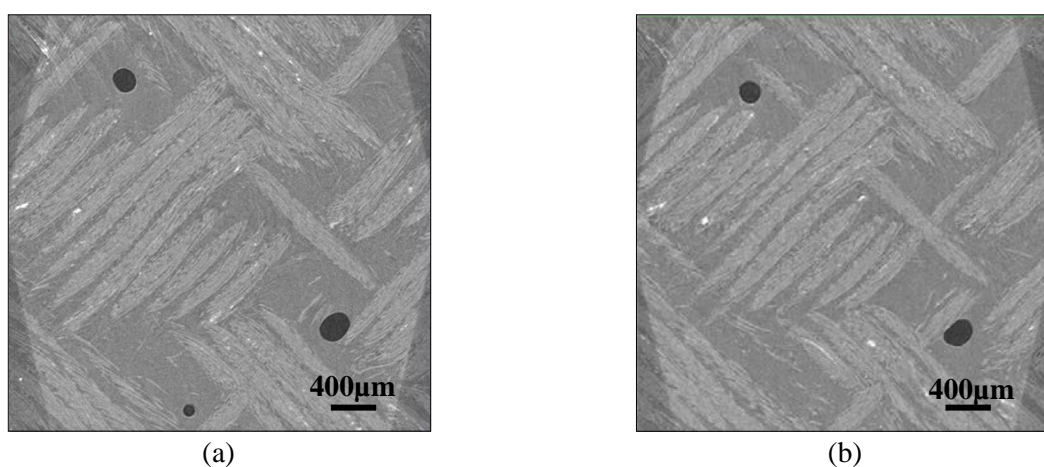


assembling of elementary fibres and technical fibres. The technical fibres are themselves composed of ~2 to 5 inseparable elementary fibres. The diameters of technical fibres and elementary fibres can be estimated by 30–300  $\mu\text{m}$  and 15–35  $\mu\text{m}$ , respectively. As it can also be seen in figure 6, elementary fibres are characterised by a lumen; an open channel in their centre. This lumen is observable in few elementary flax fibres. Not all of flax elementary fibres have a visible lumen.



**Figure 6.** Figure illustrating the different microstructural parameters in flax epoxy laminate,  $[0^\circ, 90^\circ, +45^\circ, -45^\circ]_s$  structure. (a) 2D slice in x-y plane. (b) 2D slice in x-z plane, the insert is the zoomed lumen.

A more rigorous visual inspection performed on the numerous 2D tomographs in the 3 different planes, revealed also good quality of impregnation. Moreover, matrix porosities which could not be detectable using optical microscopy were revealed by CT analysis. Yet, only very small amount of porosities was detected (figure 7).



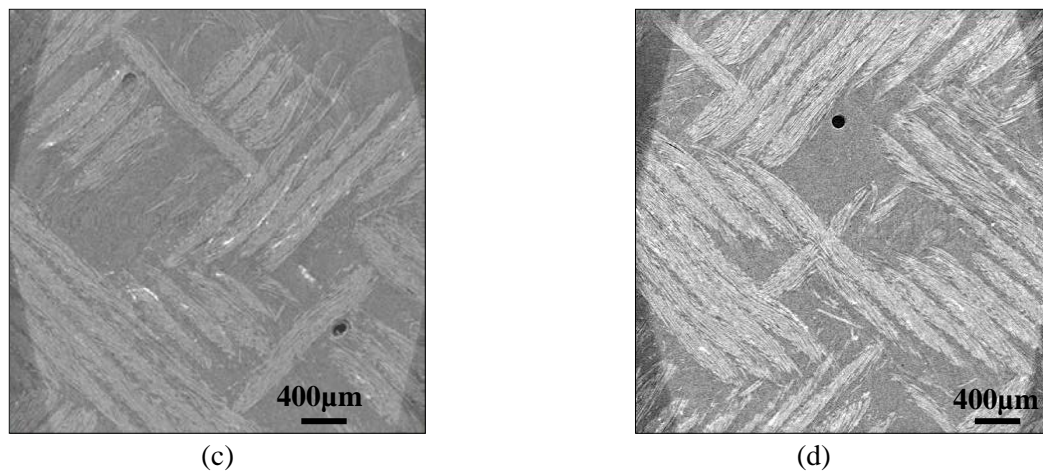


**Figure 7.** Internal 2D slices in x-z plane illustrating porosities in  $[45^\circ, -45^\circ]_{2s}$  laminate.

For the purpose of understanding how damage affects the stress-strain response of the material during loading CT method was used. Samples relative to the different studied laminates were subjected to tensile loading and then the overall stress-strain responses were established.

### 3.3 Tensile tests

The samples relative to each laminate were loaded in uniaxial tension afterwards they were subjected to CT analysis. Tensile tests were performed using an INSTRON 4505 machine with a loading capacity of 100 kN according to ASTM D3039 standard. The crosshead speed, temperature and humidity during the tests were 5 mm/min, 20°C and 50%, respectively.

**3.3.1 Stress-strain curves.** The stress-strain curves for the samples are represented in figure 8. As it can be seen the tensile test revealed a specific behaviour of the strain-stress curves, characterized by a bilinearity. Three main portions can be observed: the first (1) and the third (3) portions behave linearly and the second (2) one exhibits a non-linear behavior. On the basis of these curves, the tangent modulus ( $E$ ) degradation, during loading, was evaluated and the variation of  $E$  versus strain for one characteristic stress-strain diagram was plotted in the same graph (figure 6). As it can also be seen the non-linear behaviour is manifested at the early stage of loading in all of the studied laminates. The onset of non-linearity is in the range of 0,12%...0,2% strain for  $[0^\circ]_8$ ,  $[0^\circ, 90^\circ]_{2s}$ ,  $[0^\circ, 90^\circ, +45^\circ, -45^\circ]_s$  laminates and 0,5% strain for  $[+45^\circ, -45^\circ]_{2s}$  laminate. The onset of the non-linearity of the stress-strain curves is defined as strain for which the tangent slope of the curve is decreased by 10% of its initial value.

Young modulus and the main mechanical properties calculated on the basis of the stress-strain curves: ultimate strength, ultimate strain and Poisson ratio, identified from stress-strain curves, are listed in table 1.

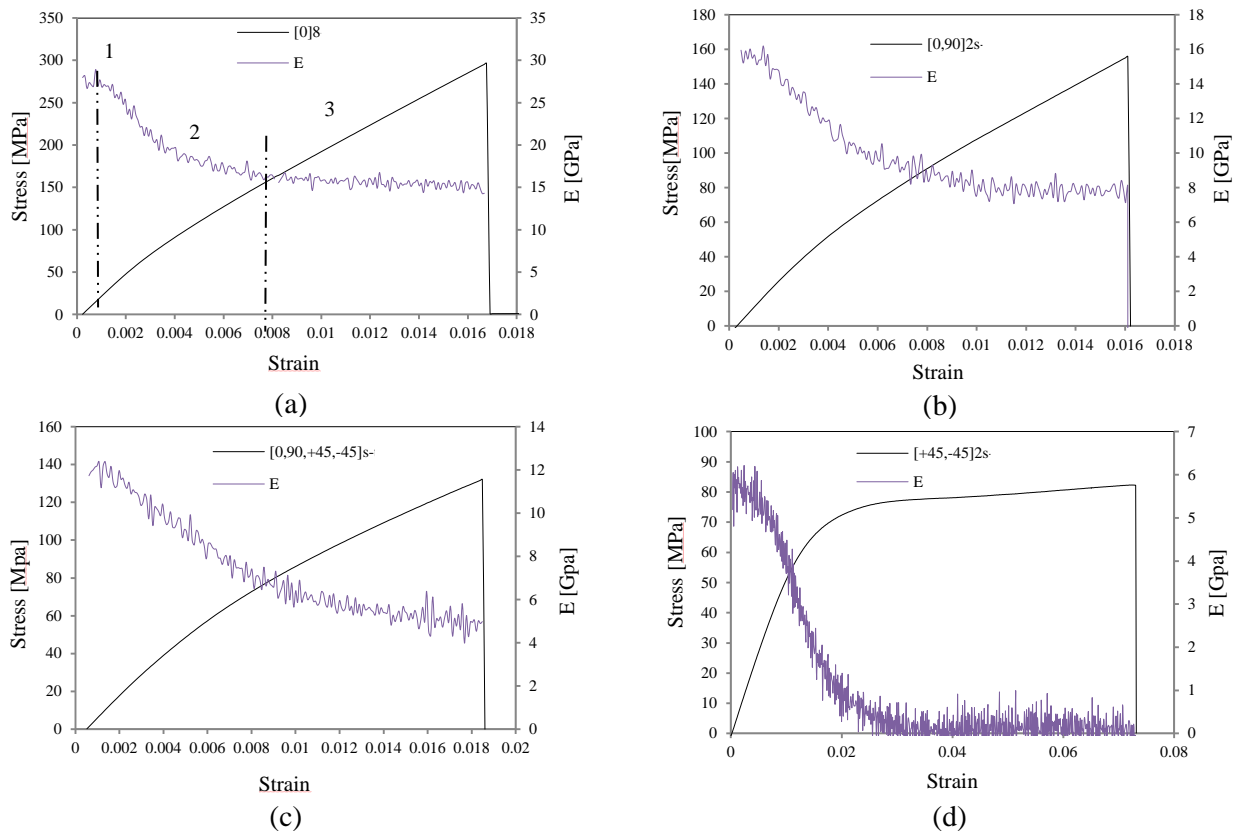


**Figure 8.** Stress–strain curves and stiffness–strain curve: (a)  $[0]_8$ . (b)  $[0^\circ, 90^\circ]_{2s}$ . (c)  $[0^\circ, 90^\circ, 45^\circ, 45^\circ]_s$ . (d)  $[45^\circ, 45^\circ]_{2s}$ .

**Table 1.** Table summing up the main tensile and AE results. Note: the scatter gives the standard deviation in three tests.

	Onset of non-linearity strain [%]	Initial Young's modulus [GPa]	Poisson's ratio	Ultimate strength [MPa]	Ultimate strain [%]
$[0]_8$	0.12	$27.2 \pm 0.52$	$0.409 \pm 0.034$	$296 \pm 0.5$	$1.65 \pm 0.055$
$[0^\circ, 90^\circ]_{2s}$	0.14	$15.7 \pm 0.15$	$0.126 \pm 0.014$	$158 \pm 2$	$1.62 \pm 0.5$
$[0^\circ, 90^\circ, 45^\circ, 45^\circ]_s$	0.2	$11.9 \pm 0.6$	$0.319 \pm 0.259$	$126 \pm 7.5$	$1.76 \pm 0.15$
$[45^\circ, 45^\circ]_{2s}$	0.5	$5.7 \pm 0.11$	$0.566 \pm 0.064$	$85 \pm 4$	$7.47 \pm 0.415$

Similar non-linearity behavior of the stress–strain curves relative to the flax fibres and flax fibre reinforced composites was also reported in refs [5,6,7]. The non-linearity phenomena which manifests at the early stage of loading is probably due to intrinsic changes of flax fibres which cause material stiffness decrease. To better understand the non-linearity phenomena and damage mechanisms which occur during loading, tensile tests were performed on another series of samples at different stages of loading. The tensile tested specimens were then subjected to CT analysis.

### 3.2 X-ray computed tomography (CT) of tensile tested samples at different stages of loading

The 3D images for the tensile tested samples were reconstructed and meticulous visual inspection was performed on ~ 2000 tomographs in each plane of the studied laminates. The analysis revealed that at

the first stage of loading, corresponding to region 2 of the stress-strain curves, microcracks are present on interface of the yarns and technical fibres. In the previous study [4] where damage was monitored by acoustic emission technique, these small cracks started from the applied strain level corresponding to onset of the AE events. Figure 9, figure 10 and figure 11 illustrate these small cracks in all the studied laminates.

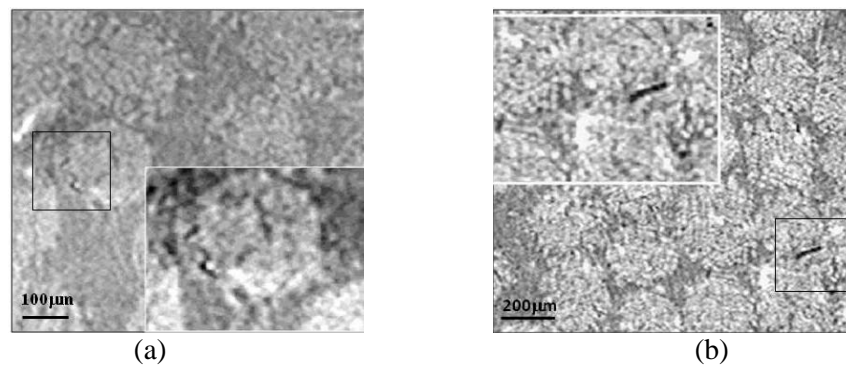


**Figure 9.** Internal 2D slice in x-z plane illustrating microcracks on (a) technical fibre interface and (b) yarn/matrix interface,  $[0^\circ]_8$  laminate. Insert, the zoomed cracked region.

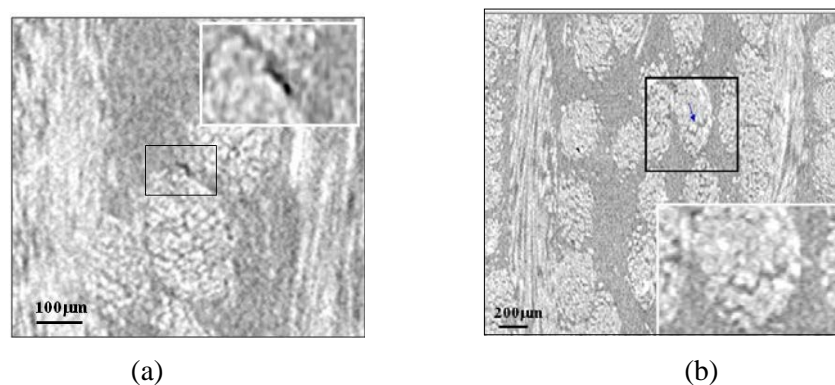


**Figure 10.** Internal 2D slice illustrating microcracks on (a) yarn/matrix interface in x-y plane,  $[0^\circ, 90^\circ]_{2s}$  laminate and (b) technical fibre interface in x-z plane,  $[0^\circ, 90^\circ, +45^\circ, -45^\circ]_s$  laminate. Insert, the zoomed cracked region.

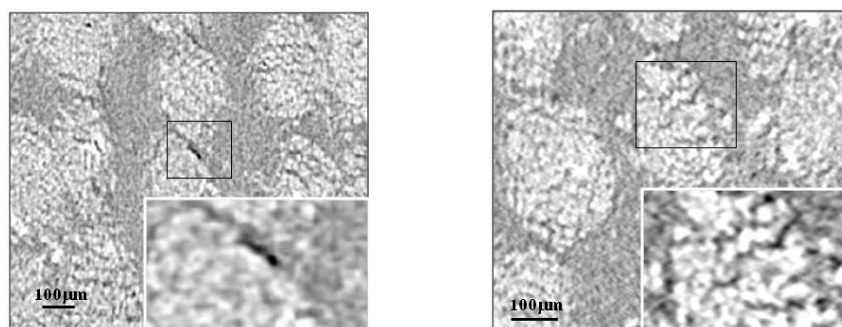


**Figure 11.** Internal 2D slice illustrating microcracks in x-z plane,  $[+45^\circ, -45^\circ]_{2s}$  laminate. (a) on yarn/matrix interface (b) On the technical fibre interface. Insert, the zoomed cracked region.

As the loading increases, these microcracks may growth and developed. Here (figure 12) we present an image where cracks are well illustrated, when load is increased.



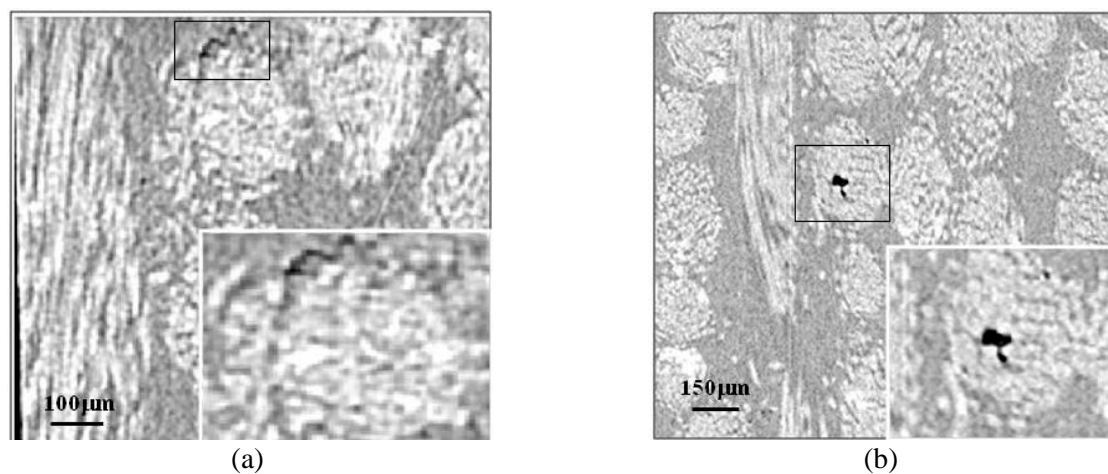


**Figure 12.** Internal 2D slice in a scanned 3D volume,  $[0^\circ, 90^\circ, +45^\circ, -45^\circ]$ s laminate (a) crack is seen at the interface of the yarn, x-y plane (b) shows crack at the technical fibre interface, x-z plane. Insert the zoomed cracked part.

The low adhesion of epoxy resin to flax fibres could favorite the occurrence of cracks on the interfaces of yarns. The presence of a relatively considerable number of lumens in the technical fibre could also stimulate the development of cracks on the technical fibres interfaces [3].

#### 4. Conclusion

The 3D X-ray computed tomography technique allowed us to visualise the external and internal of 3D microstructures. This method was used to characterise four types of laminates. CT analysis complements and corroborates previous study made on similar laminates: The visual inspection performed on numerous tomographs in the different planes (x-y, x-z and z-y) of the damaged samples showed that cracks seem to be located at yarn-matrix and technical fibre interfaces in all stages of loading. Moreover, 3D X-ray tomography revealed also the observed absence of the transverse matrix cracking not only at the external surface level but in all the internal structure of the material. The absence of such cracks can be a major advantage for the use of natural fibre reinforced composites. Even though, CT method enriches the results but how damage affects the stress-strain response of the material remains still not fully understandable. More work should then be also undertaken in future studies.

#### References

- [1] Slattery ATI, 1936, Some observations on the size and shape of the flax fibre ultimates, *J.Text. Inst Trans* **27** T101–T108
- [2] CELC, 2012, *Flax and Hemp fibres: a natural solution for the composite industry* (Paris: JEC Composites)
- [3] Barley C, Perrot Y, Busnel F, et al, 2006, Transverse tensile behaviour of unidirectional plies reinforced with flax fibres, *Mater Lett* **60** 2984–87
- [4] Kersani M, Lomov SV, Van Vuure AW, et al, 2015, Damage in flax/epoxy quasi-unidirectional woven laminates under quasi-static tension *J Compos Mater* **49** 403–13
- [5] Baley C, 2002, Analysis of the flax fibres tensile behaviour and analysis of the tensile stiffness increase, *Compos Part A* **33** 939–48
- [6] Charlet K, Eve S, Jernot JP, et al, 2009, Tensile deformation of a flax fiber, *Procedia Eng* **1** 233
- [7] Hughes M, Carpenter J and Hill C, 2007, Deformation and fracture behaviour of flax fibre reinforced thermosetting polymer matrix composites, *J Mater Sci* **42** 2499–511